Relationship between solar wind, D_{st}, and plasmasphere mass density on one-hour time scales

Victoir Veibell[*] R.S. Weigel[†]

September 1, 2015

Abstract

This paper compares various magnetosphere conditions around the onset of geomagnetic events. It confirms results from previous papers that a sudden drop in D_{st} correlates with a spike in equatorial mass density under certain conditions, while adding a level of depth and specification to the applicability of their results. It compares data at 1-hour averages to data at 1-day averages to examine if the trend holds at varying time scales and finds that it does, so long as the data is pre-processed to linearly remove a large time scale $F_{10.7}$ dependence. By then looking at an hourly average of parameters from 24 hours before event onset to 48 hours after, short timescale trends can be discerned.

1 Introduction

Takahashi et al. [2006], show how trends in storm dependence on mass/density only appear in longer timescales. Looking at K_p vs mass (amu) in the range of 6 to 7 R_E, a trend shows up in the 1.5 day averages that doesn't appear in the 3 hour averages.

Denton et al. [2006] show how D_{st} affects the distribution of plasma density along different magnetic latitudes, and specifically along the same field lines as looked at in later papers (6-8R_E). Though this shows that the trends for density may differ between field lines, it's mentioned mostly as a point for future research as the data used in this paper is already adjusted for one field line, as described by Takahashi et al. [2010].

Yao et al. [2008] looks at the differences in how D_{st} correlates with number density for different ions in different regions (ring current and plasma sheet), but still finds a general correlation during each of the four storms selected.

Takahashi et al. [2010] state that spikes in the Disturbance Storm Time (D_{st}) index coincide with with significant changes in ρ_{eq} at an L-shell of $6.8R_E$. For five storms over a 20 day period two had ρ_{eq} spikes after the D_{st} drop, two had ρ_{eq} spikes before the drop, and one showed little change in ρ_{eq}. They then show an epoch analysis where ρ_{eq} is seen to spike the day of a D_{st} drop, using a daily average of 30 minute ρ_{eq} and one hour D_{st} measurements.

2 Data Preparation

The parameters ρ_{eq} used in this work is from the dataset associated with Denton [2007], with data available from 1980-1991 on a non-uniform 10 minute grid. The $F_{10.7}$ parameter comes from the OMNIWeb data collection at NASA Goddard Space Flight Center and covers 1980-2000 on an hourly grid, but with one daily value repeated for each hour of the day. All other parameters are from Kondrashov et al. [2014] over the time range of 1972-2013, which are on a 1-hour time grid. ρ_{eq} is the inferred mass density based on the 3rd harmonic frequency of magnetic field measurements. The smallest cadence for ρ_{eq} values is 10 minutes. To compute an hourly average over the same time range as the solar wind parameters, the median of all values in a given hourly range was used. Fill values were used for hours when no measurements were available. In cases where ρ_{eq} was available from multiple Geostationary Operational Environmental Satellites (GOES) satellites at the same time in the Denton [2007] dataset, the value from GOES 6 was selected to avoid overlapping data points. In the dataset, measurements from GOES 6 had the longest time span of coverage. An overview of the data is given in Figure 1.

[*]vveibell@gmu.edu
[†]rweigel@gmu.edu

In this work events are defined to occur when D_{st} or ρ_{eq} crosses a threshold value, as indicated in by horizontal dashed lines in the respective panels of Figure 1. In finding events, all fill values were replaced with linearly interpolated values. Figure 1 shows the values of B_z, V_{SW}, D_{st}, $F_{10.7}$, and Mass Density for the duration of the dataset.

3 Results

Figure 1 shows values of solar wind averages and mass density used in this study. We will briefly compare our results to other published results to verify our methods and handling of data.

3.1 Previous Results

Figure 2a shows the long-term trends of $log(\rho_{eq})$ and $F_{10.7}$ by computing the median in 27-day windows using all non–fill hourly values. A scatter plot of these two lines is shown in Figure 2b. The linear correlation is found to be 0.87. In comparison, Takahashi et al. [2010] found a correlation coefficient of 0.94 using measurements from all satellites in the time interval of 1980 to 1992.

The correlation seen between 27-day averages $log(\rho_{eq\_27d})$ and $F_{10.7\_27d}$ isn't quite as good in this data as in Takahashi et al. [2010], but shows the same trend as seen in Figure 2.

Figure 3 show that the trends observed by Takahashi et al. [2010] for one day averages only seems to hold true for the one-day averaged data. Namely that a drop in median daily D_{st} between 1989 and 1991 coincides with a significant spike in ρ_{eq}.

3.2 D$_{st}$ Events

Two event indicators are looked at in this study. The first is looking for a drop in DST below the threshold of $-40nT$ specified in Takahashi et al. [2010], dubbed the "onset", and then considering the timeframe an event until D_{st} passes back above the $-40nT$ threshold. This method finds 669 such periods between May 1983 and August 1991 with an average duration of 9 hours and a median duration of 3 hours. Figure 5 shows the average values of all events over a window of 24 hours before onset and 48 hours after. Figure 5a shows events selected by looking for event onsets where D_{st} crossed a threshold of $-40nT$. The dashed red lines indicate plus and minus one standard deviation of values from all events that went into the average. The final plot in the stack shows both ρ_{eq} and a bar plot of how many valid data points went into the ρ_{eq} average. Since ρ_{eq} comes from a sparser dataset, it has less valid points contributing to the averages than the other parameters in the stack. A subset of longer duration events will be looked at later.

This figure shows a definite spike in the Z component of the magnetic field, as well as the defined drop in DST, but no obvious change in mass density at an hourly timescale. This points to an issue with only looking at long-timescale trends between density and D_{st}, and allows for the possibility that other factors are influencing the long term correlation since there's no obvious connection on a short timescale. One possibility is that, as suggested in Takahashi et al. [2010], $F_{10.7}$ plays a significant role in driving long term density values which biases the long term correlation of density and D_{st}.

3.3 Mass Density Events

Figure 5b shows this same algorithm, but looking for a rise in mass density over a value of $40g/cm^3$. This results in 130 events with a mean duration of 32 hours and a median duration of 17 hours, marked in red on the left figure.

This shows that when using all data for mass density derived events, almost no significant changes can be seen around event onset.

4 More specific events

It's hypothesized that progressively picking more specific event criteria will allow for the possibility of more significant results, at the expense of more bias in the selection process and potentially less overall usefulness of the results. That said, the predictability of extreme events is of definite interest, so an attempt has been made to find some reproducible method of prediction. Looking at events that last longer than 12 hours and events with an onset threshhold greater than $70g/cm^3$ results in the left and right sides of Figure 6 respectively.

Neither of these seem to indicate anything too significant, so looking at D_{st} events instead to look for something that causes a significant change in Mass Density results in Figure 7. This shows that by either looking only at D_{st} events that last longer than an hour (left) or at events where the onset condition is $D_{st} < -80nT$, a spike in mass density is seen, but also a definite lack of data availability to the point where that spike may be coming from less than five of the total 143 events.

Unfortunately there are no events in this time frame that are longer than 12 hours with D_{st} minima lower than $-80nT$ that have existing mass density data around onset, so an analysis of this particular relationship can't be made.

4.1 Change in ρ_{eq}

If instead of looking for events based on a threshold of ρ_{eq}, we instead look for a certain amount of change in ρ_{eq} as the basis for event onset, we get Figure 8.

Both raw change and percent change were done in case of bias towards high or low ρ_{eq} periods, respectively. This shows a distinct lack of correlation in either case to a change in D_{st}. The percent change in ρ_{eq} does, however, seem to be preconditioned by changes in B_z and $F_{10.7}$.

5 F10.7 dependence

In an effort to analyze the dependence of ρ_{eq} on $F_{10.7}$, a few tests were performed. Takahashi et al. [2010] mention a strong correlation between the two. The long term correlation could be a bias for D_{st}'s effects, so a linear model was created, recreating mass density purely from $F_{10.7}$ in the form of $\rho_{eq}(t) = A * F_{10.7}(t)$. This re-created ρ_{eq} shows around a 45% correlation with the actual ρ_{eq}, suggesting a strong influence, while doing the same procedure with DST shows only a 20-25% correlation.

Taking this re-created data set and subtracting it from the original should remove the $F_{10.7}$ dependence from the data, and allow for a less biased analysis of the relationship between D_{st} and ρ_{eq}. Figure 9 shows the stack plot for the reduced $F_{10.7}$, where a more distinct peak after event onset can be seen. It also shows what that removed trend looks like, of the form $\rho_{eq} - \rho_{eq,F_{10.7}}$.

6 Appendix

6.1 Bias

While attempting to reproduce Figure 11 from Takahashi et al. [2010], an ambiguity in data-handling was found. It is unknown how they got from hourly ρ_{eq} to daily medians, whether in one step or two steps, and whether the hourly medians are an hour ahead of each hour grid point, or a median of points a half hour to either side, so attempts were made to reproduce all possibilities and compare in order to find a data-handling method with the least bias. These attempts are shown in Figure 10. This also shows the effect of only considering events with a minimum before noon. All show a similar spike in ρ_{eq} at the time of D_{st} minimum, though none quite reproduce the exact values seen in Takahashi et al. [2010]. Figure 11 shows where the median falls for all of the found events during that period, as a sanity check for why the prior work would get median values nearing $30amu/cm^3$. Both authors of this paper conducted independent trials to confirm that the data and analysis don't quite yield the results of Figure 11 in Takahashi et al. [2010] with the processes described in that paper, but the same general trend is still seen.

To check for potential bias in the data as used by our analysis, we checked how the data availability varied with hour, shown in Figure 12. We also looked at how storm conditions affected data availability. Both a two sample t-test for difference in means and a Wilcoxon rank sum test showed significance at the 1% level that D_{st} during periods with available data was of a different distribution than D_{st} during periods missing data. When testing for other significant D_{st} differences, the Wilcoxon test was significant while the t-test was not in pre-noon vs post-noon distributions, as well as $\rho_{eq} > 40$ vs $\rho_{eq} < 40$ distributions indicating perhaps an increase in variability without an increase in mean.

While the GOES Satellites tend to keep an average geostationary distance of around $L = 6.8R_E$ shown in Takahashi et al. [2010], the actual plasmapause location varies significantly, as shown in O'Brien and Moldwin [2003]. This means that during periods of large D_{st} the plasmapause may be far from the point of measurement of ρ_{eq} creating a discord in the correlation. Gallagher et al. [2000] provides a model for ρ_{eq} at a range of L-shells and a brief discussion of the elemental contributions.

References

K. Takahashi, R. E. Denton, R. R. Anderson, and W. J. Hughes. Mass density inferred from toroidal wave frequencies and its comparison to electron density. *Journal of Geophysical Research (Space Physics)*, 111:A01201, January 2006. doi:10.1029/2005JA011286.

R. E. Denton, K. Takahashi, I. A. Galkin, P. A. Nsumei, X. Huang, B. W. Reinisch, R. R. Anderson, M. K. Sleeper, and W. J. Hughes. Distribution of density along magnetospheric field lines. *Journal of Geophysical Research (Space Physics)*, 111:A04213, April 2006. doi:10.1029/2005JA011414.

K. Takahashi, R. E. Denton, and H. J. Singer. Solar cycle variation of geosynchronous plasma mass density derived from the frequency of standing Alfvén waves. *Journal of Geophysical Research (Space Physics)*, 115:A07207, July 2010. doi:10.1029/2009JA015243.

Y. Yao, K. Seki, Y. Miyoshi, J. P. McFadden, E. J. Lund, and C. W. Carlson. Effect of solar wind variation on low-energy O+ populations in the magnetosphere during geomagnetic storms: FAST observations. *Journal of Geophysical Research (Space Physics)*, 113, 2008. doi:10.1029/2007JA012681.

R. Denton. Database of Input Parameters for Tsyganenko Magnetic Field Models, 2007. URL `http://www.dartmouth.edu/~rdenton/magpar/index.html`. Retrieved 2013-10-28.

NASA Goddard Space Flight Center. Omniweb. URL `http://omniweb.gsfc.nasa.gov/form/dx1.html`. Retrieved 2015-06-11.

D. Kondrashov, R. Denton, Y. Y. Shprits, and H. J. Singer. Reconstruction of gaps in the past history of solar wind parameters. *Geophysical Research Letters*, 41:2702–2707, April 2014. doi:10.1002/2014GL059741.

T. P. O'Brien and M. B. Moldwin. Empirical plasmapause models from magnetic indices. *Geophysical Research Letters*, 30:1152, February 2003. doi:10.1029/2002GL016007.

D. L. Gallagher, P. D. Craven, and R. H. Comfort. Global core plasma model. *Journal of Geophysical Research*, 105:18819, August 2000. doi:10.1029/1999JA000241.

7 Figures

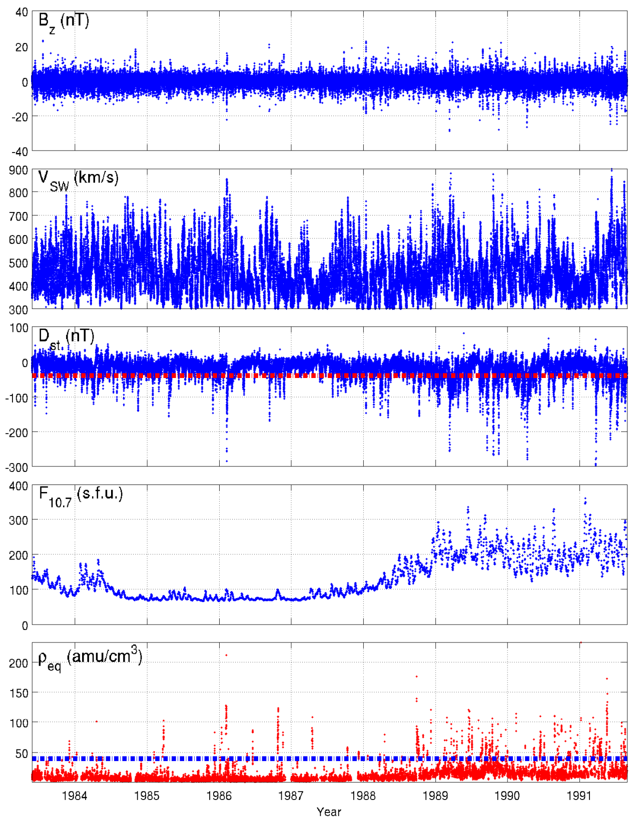

Figure 1: Overview of data used in this study. The top four panels show parameters from Kondrashov et al. [2014] and the bottom panel is based on ρ_{eq} from Denton [2007] after interpolation and averaging described in the text. Dashed horizontal lines in the D_{st} and ρ_{eq} panels indicate sample event cutoff thresholds of $D_{st} = -50\ nT$ and $\rho_{eq} = 40\ amu/cm^3$.

(a)

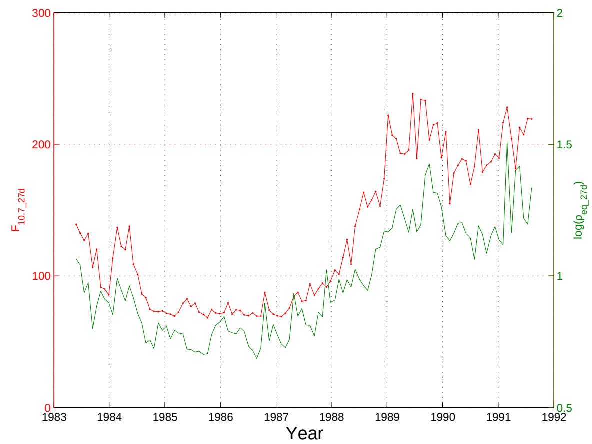

(b)

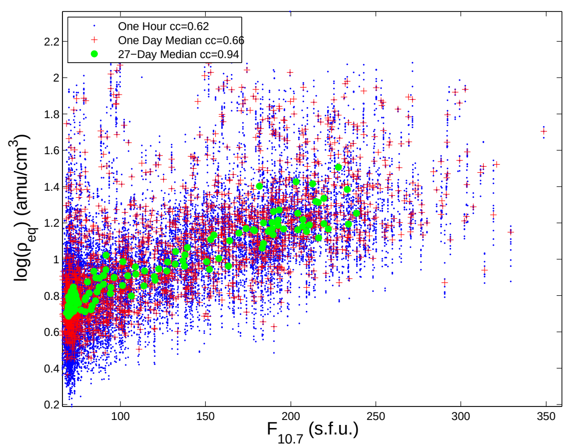

Figure 2: (a) All data of $F_{10.7\_27d}$ and ρ_{eq_27d}. (b) Correlation between $log(\rho_{eq})$ and $F_{10.7}$ at hour, day, and 27-day intervals; compare to Takahashi et al. [2010] Fig. 14

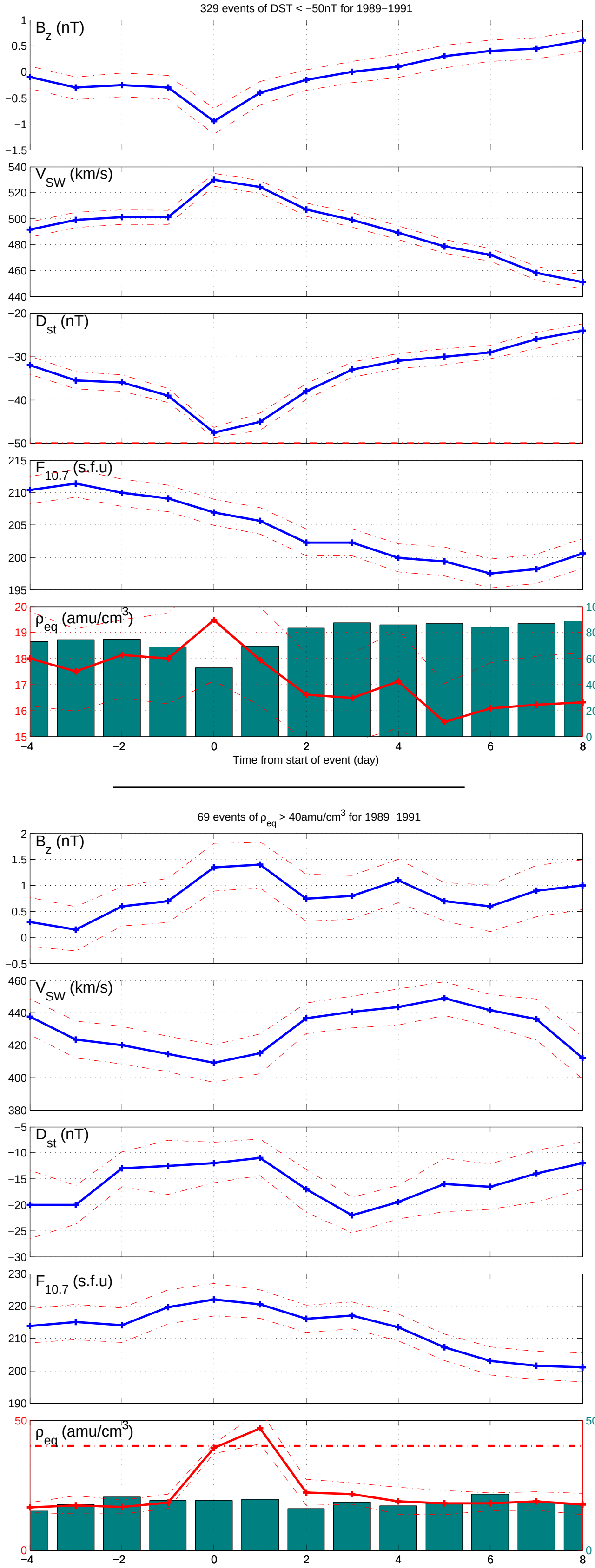

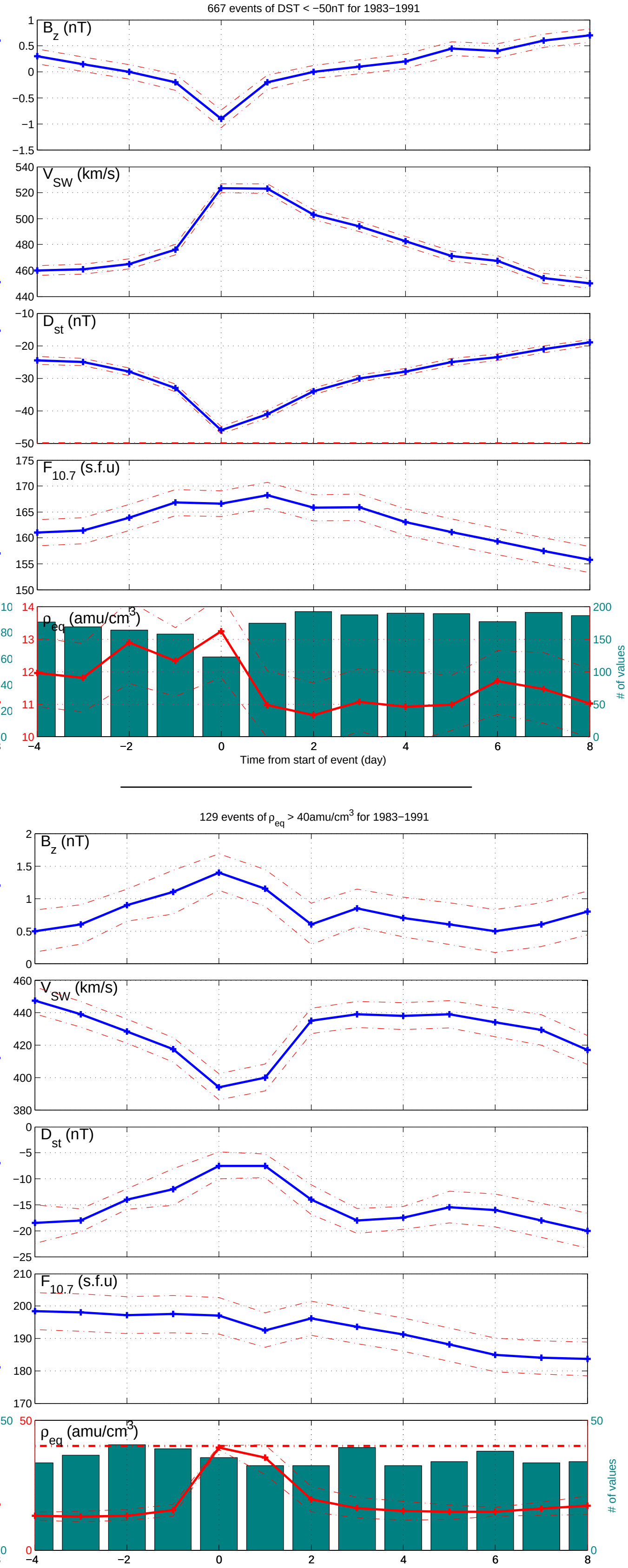

Figure 3: (a) Verifying Takahashi et al. [2010] Fig. 11 conditions: $D_{st} < -50nT$ between 1989 and 1991 and (b) Same as (a) but for ρ_{eq} events

Figure 4: Daily averages for all events in full time range for (a) $D_{st} < -50\ nT$ events and (b) $\rho_{eq} > 40\ amu/cm^3$ events

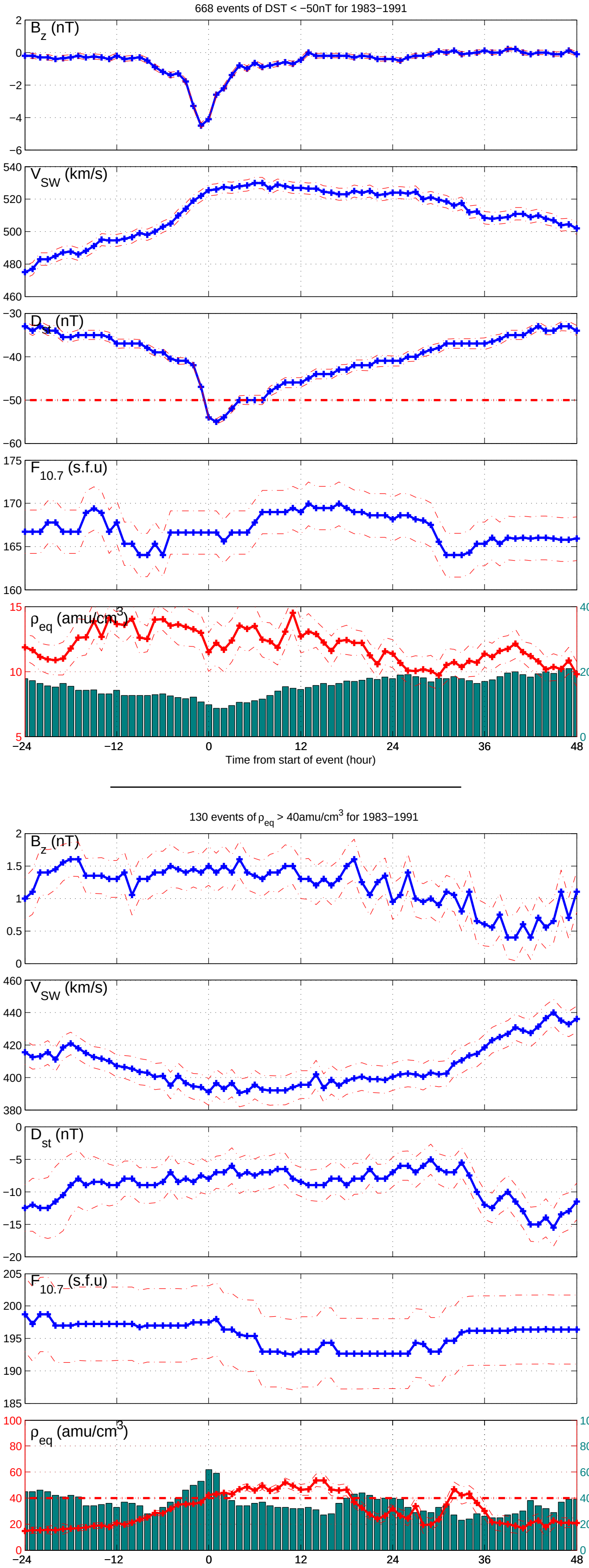

Figure 5: (a) Average of solar wind and near-Earth measurements around the time D_{st} crossed below -50 nT onset. (b) Same as (a) except around time intervals where mass density crossed above 40 amu/cm^3. The bottom panel shows the number of mass density data points that were used for the

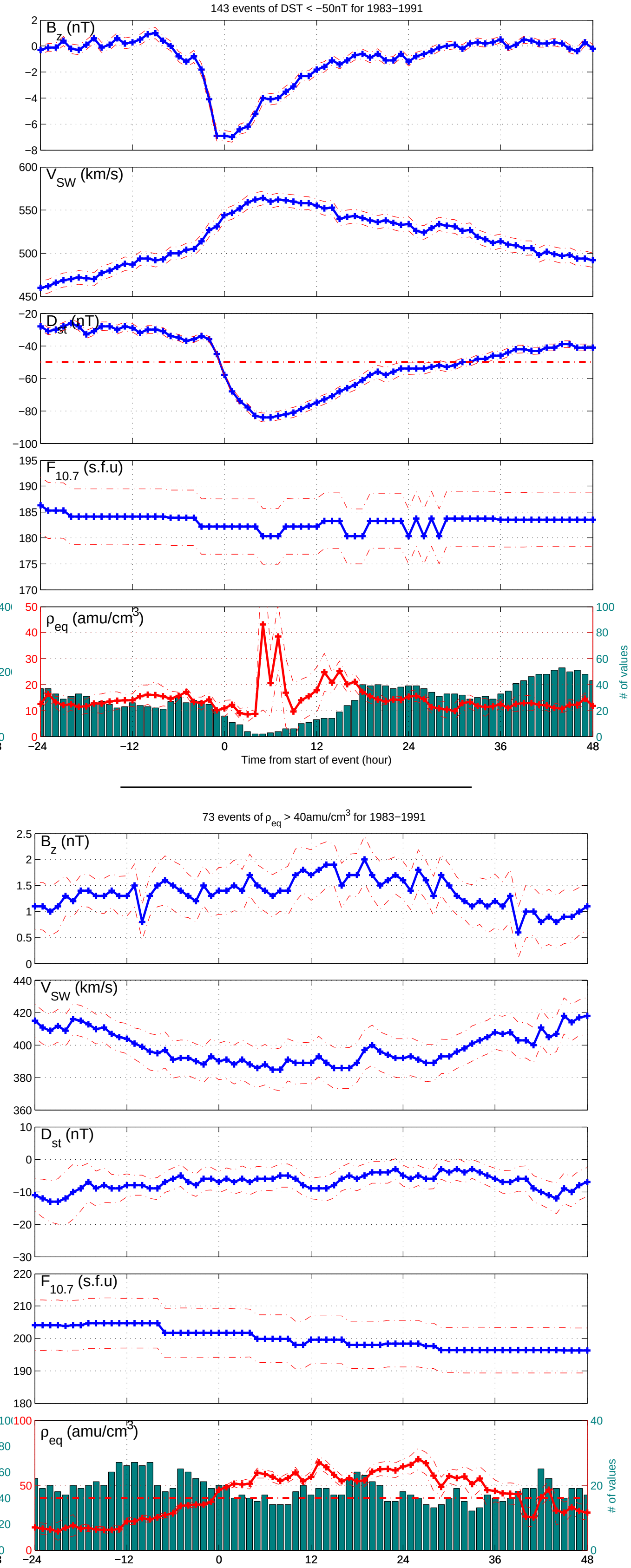

Figure 6: (a) Same as Figure 5(a) except with constraint that D_{st} stayed below -50 nT for at least 12 hours. (b) Same as Figure 5(b) except for constrain that ρ_{eq} stayed above 50 amu/cm^3 for at least 12 hours.

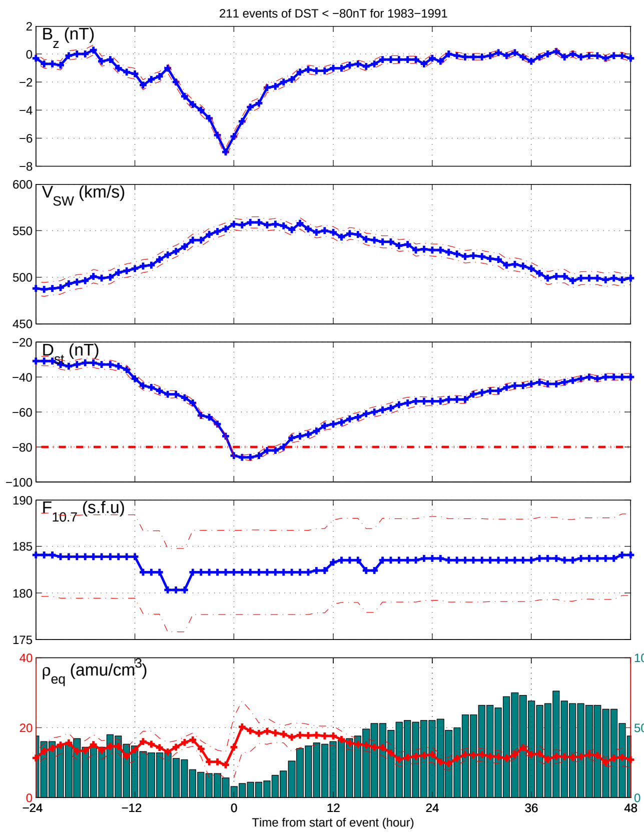

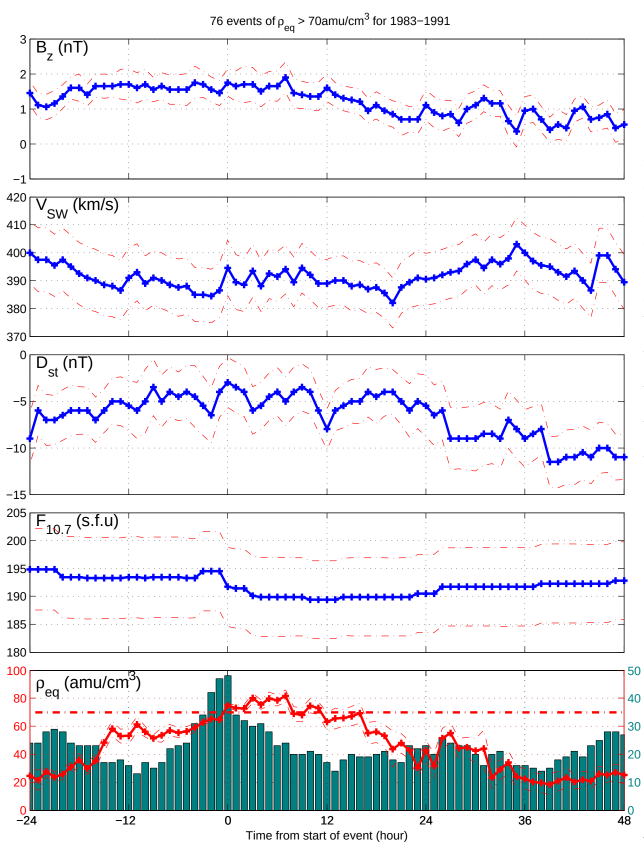

Figure 7: (a) Same as Figure 5(a) except with constraint that D_{st} crossed below $-80nT$ (b) Same as Figure 5(b) except for constrain that ρ_{eq} crossed above 70 amu/cm^3.

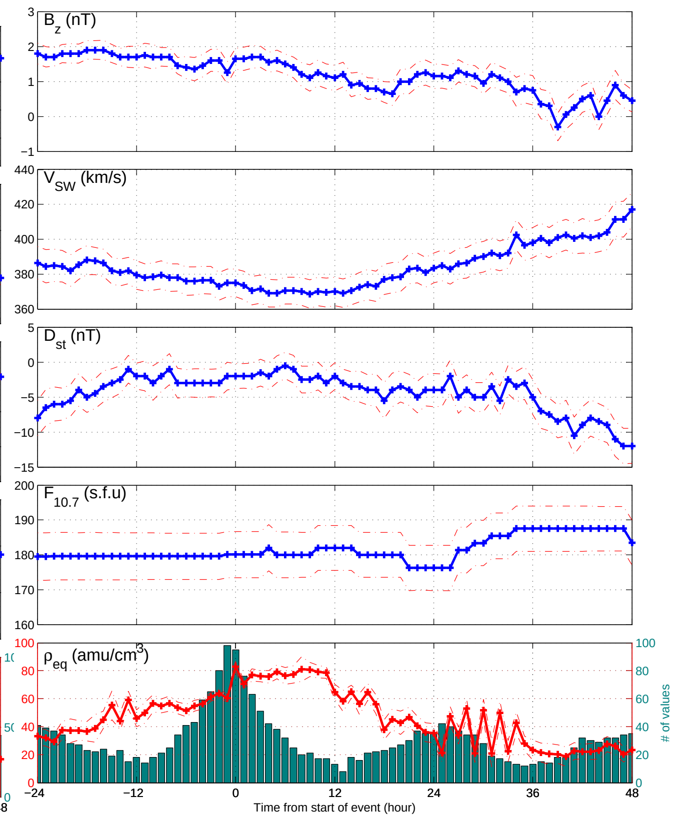

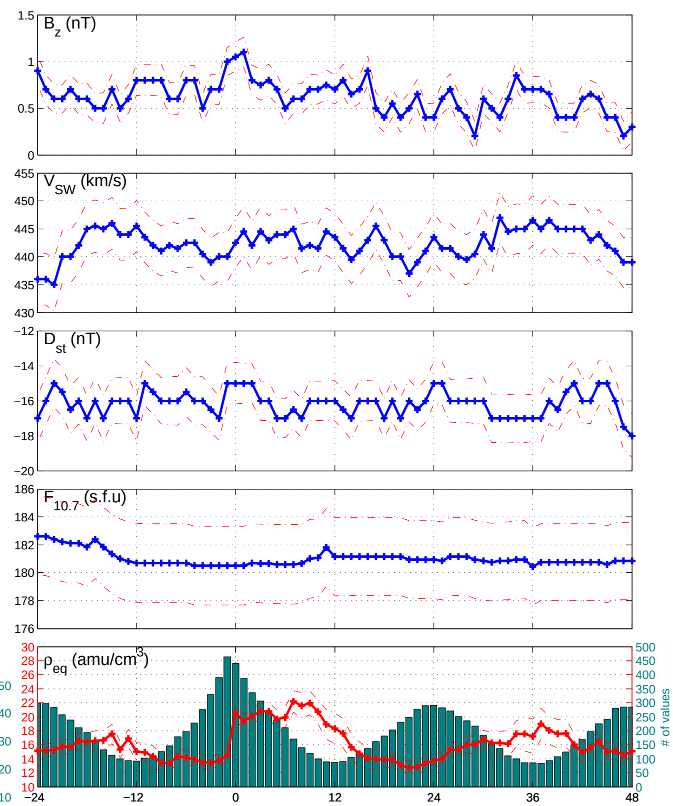

Figure 8: (a) diff(ρ_{eq}) > $10\frac{amu}{hour}$. (b) diff(ρ_{eq}) > $30\frac{\%}{hour}$

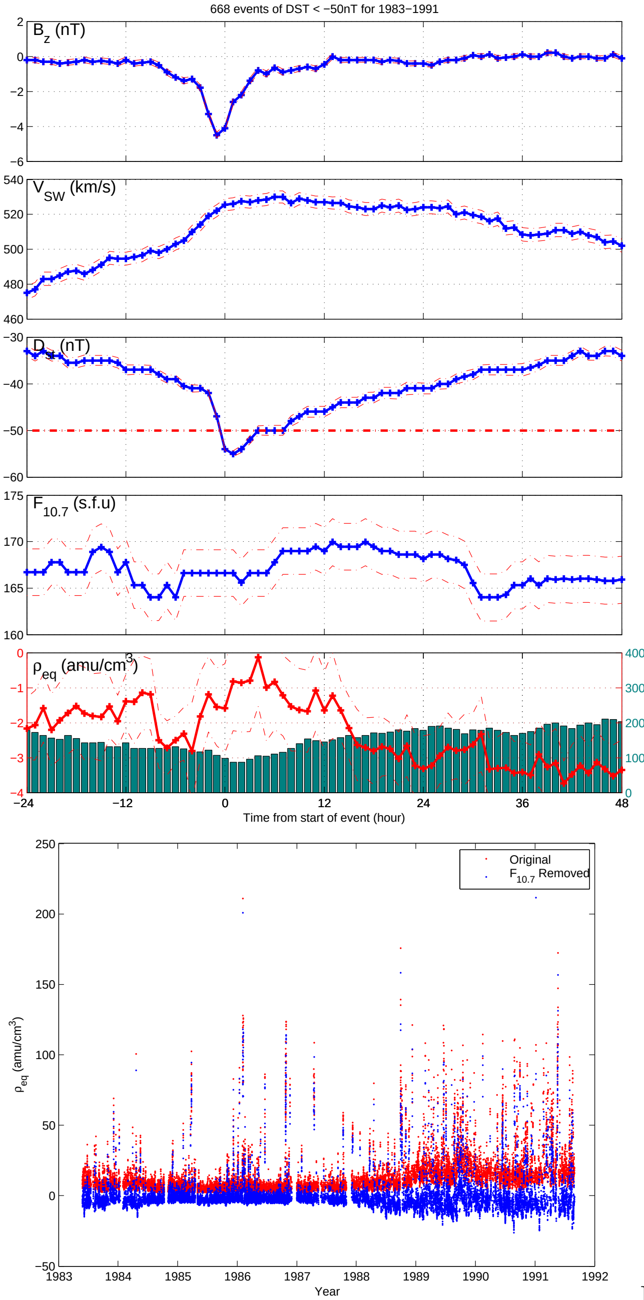

Figure 9: D_{st} events where ρ_{eq} has $F_{10.7}$ dependence removed, and Difference between original ρ_{eq} and $F_{10.7}$-less ρ_{eq}

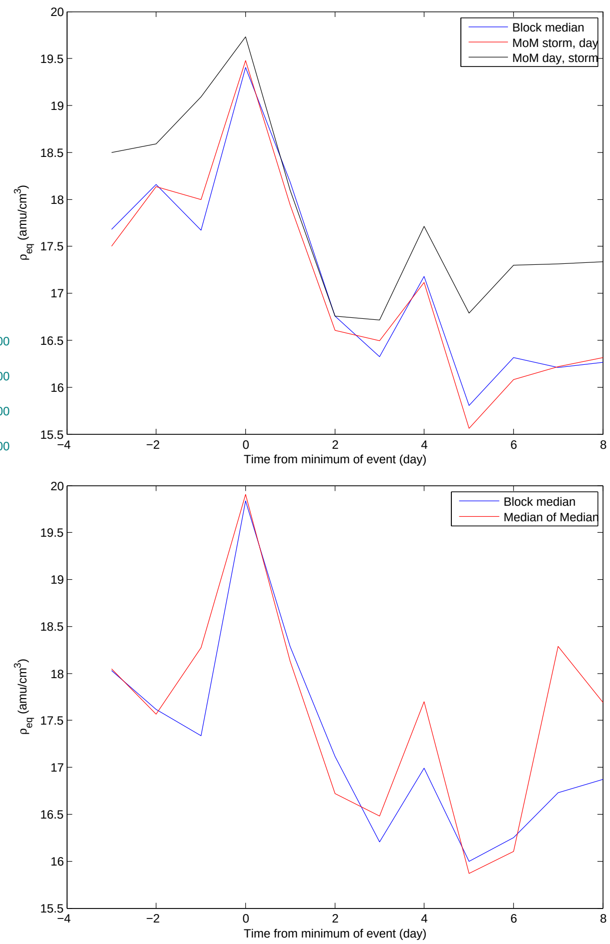

Figure 10: Comparing median values calculated as median of all 1-hour points in the 12 day block, and as the daily median of all hourly-mediated events. (b) Same, but only events starting between 0-12 UTC

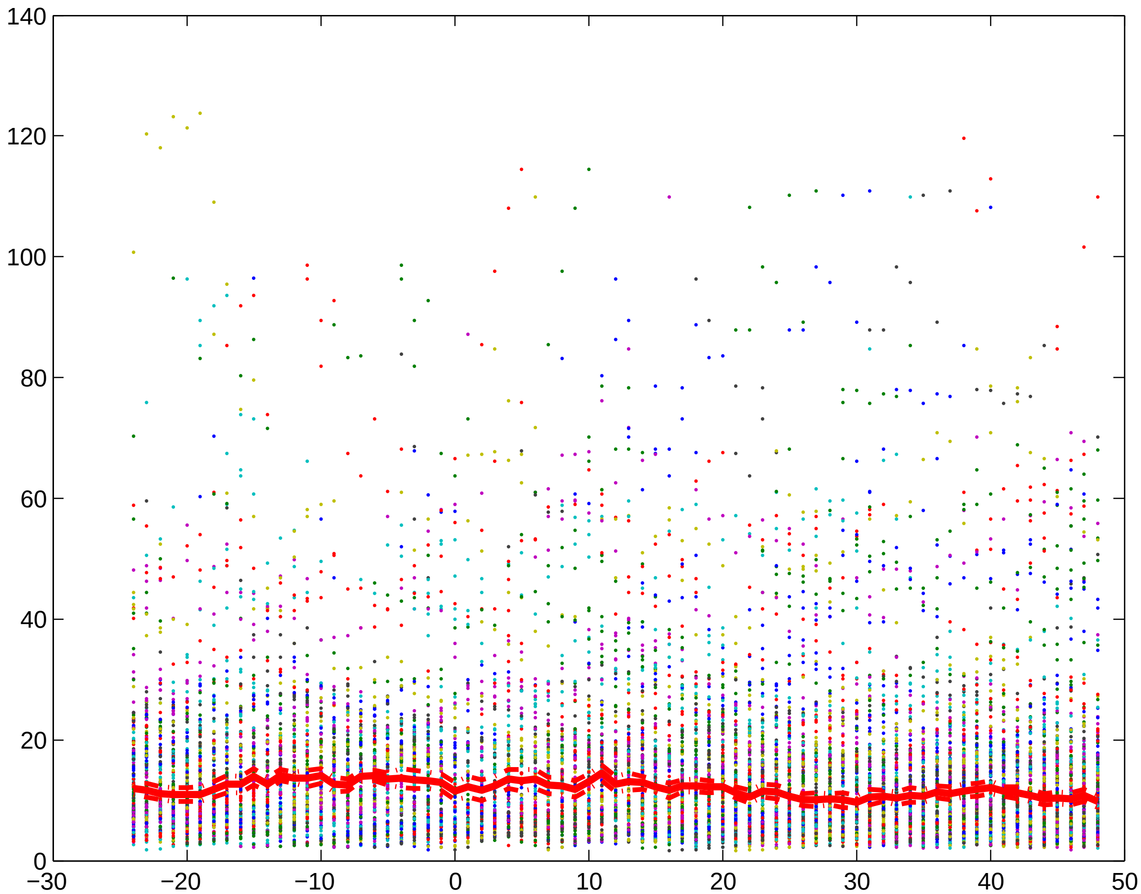

Figure 11: Comparing all events to their median and 1σ range

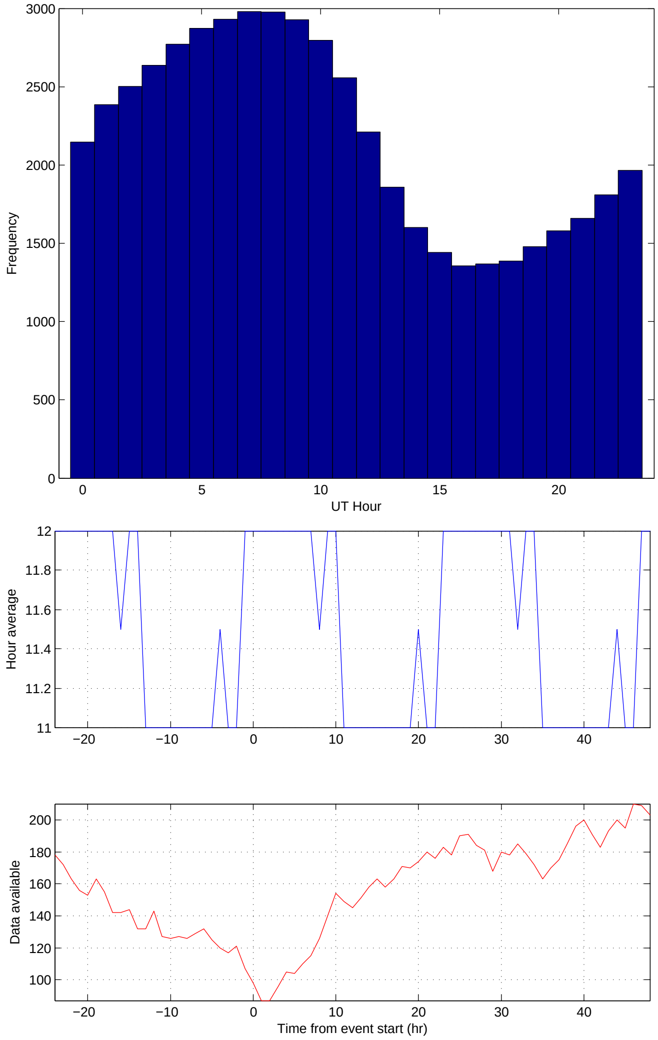

Figure 12: (a) Number of NaN points per hour of observation in the total data set (b) ρ_{eq} data availability relative to average event hour in events where $D_{st} < -80nT$